Supplementary Information

Mn-doped Co_3O_4 for Acid, Neutral and Alkaline Electrocatalytic Oxygen Evolution Reaction

Ana Luisa Silva[1], Laura M. Esteves[3,4], Ludmila P. C. Silva[3], Vitor S. Ramos[2,5], Fabio B. Passos[3], Nakédia M. F. Carvalho[1,*]

[1] Departamento de Química Geral e Inorgânica, Universidade do Estado do Rio de Janeiro, Rio de Janeiro, RJ, Brasil, 20550-900.

[2] Departamento de Engenharia Mecânica, Universidade do Estado do Rio de Janeiro, Rio de Janeiro, RJ, Brasil, 20940-903.

[3] Departamento de Engenharia Química e de Petróleo, Universidade Federal Fluminense, Niterói, RJ, Brasil, 24210-240.

[4] LAQV/REQUIMTE, Departmento de Química, NOVA School of Science and Technology, FCT NOVA, 2829-516 Caparica, Portugal.

[5] Instituto de Macromoléculas Professora Eloisa Mano, Universidade do Rio de Janeiro, Rio de Janeiro, RJ, Brasil, 21941-598.

Summary

S.1. Electrocatalysts characterization

S.1.1. X-ray diffractometry and Rietveld refinement

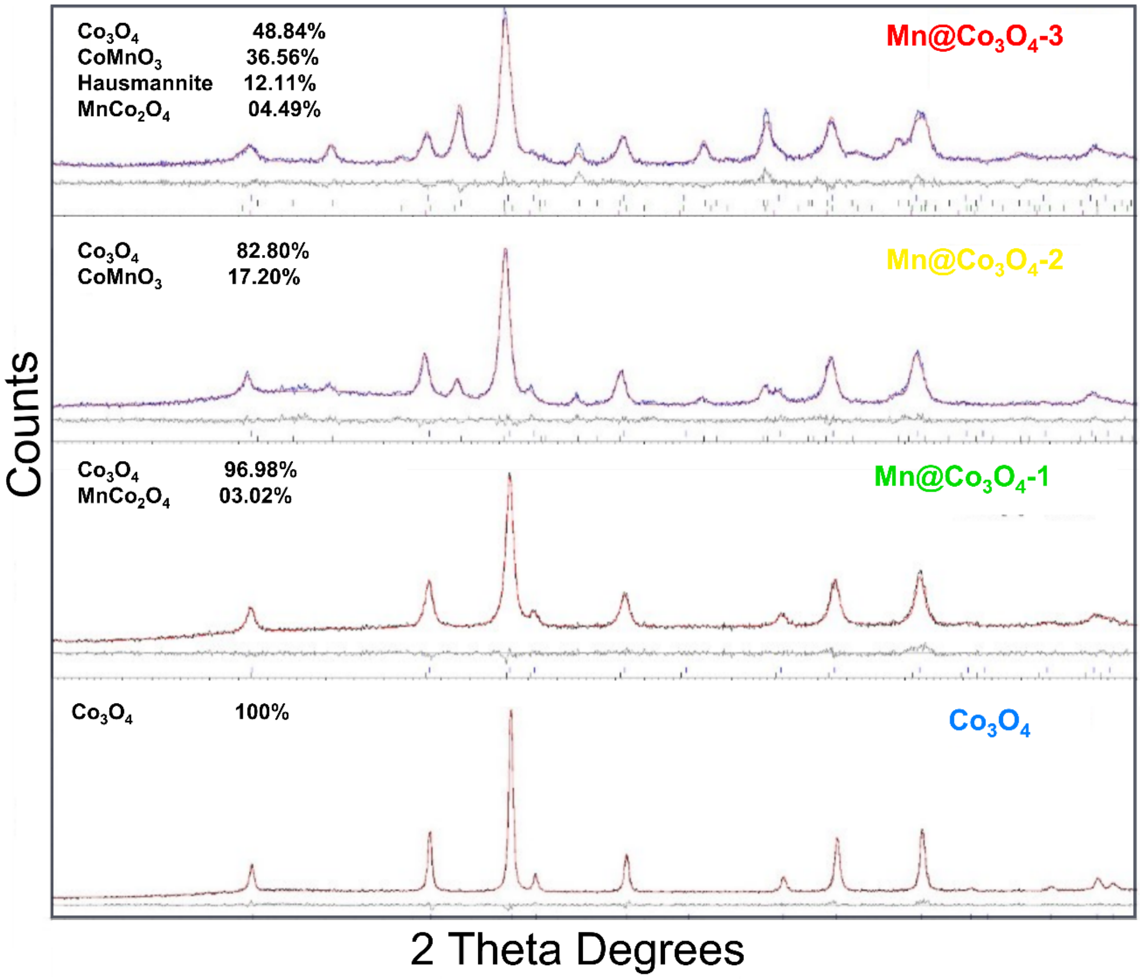

Figure S1. XRD Rietveld refinement results for: Mn@Co_3O_4-3, Mn@Co_3O_4-2, Mn@Co_3O_4-1, and Co_3O_4.

Table S1. XRD Rietveld refinement results for: Mn@Co_3O_4-1, Mn@Co_3O_4-2, and Co_3O_4.

Quantitative Analysis - Rietveld (%)							
	Co(II/III)	Mn(II),Co(IV)	Mn(II),Co(III)	Mn(II/III)	Mn/Co	Co/Mn	Co NOx
Samples	**Co_3O_4**	**$CoMnO_3$**	**$MnCo_2O_4$**	**Mn_3O_4**	**Weighted**		
Co_3O_4	100.000	-	-	-	-	-	2.7
Mn@Co_3O_4-1	96.980	-	3.02	-	0.010	96.7	2.6
Mn@Co_3O_4-2	82.800	17.200	-	-	0.094	10.7	2.9
Mn@Co_3O_4-3	46.844	36.560	4.486	12.110	0.48	2.1	2.8

Crystallite size (nm)				
Samples	**Co_3O_4**	**$CoMnO_3$**	**$MnCo_2O_4$**	**Mn_3O_4**
Co_3O_4	50.000	-	-	-
Mn@Co_3O_4-1	19.400	-	13.600	-
Mn@Co_3O_4-2	16.100	17.800	-	-
Mn@Co_3O_4-3	16.000	16.600	6.100	18.200

Cell Volume (Å^3)				
Samples	**Co_3O_4**	**$CoMnO_3$**	**$MnCo_2O_4$**	**Mn_3O_4**
Co_3O_4	529.302	-	-	-
Mn@Co_3O_4-1	533.429	-	544.053	-
Mn@Co_3O_4-2	535.586	97.070	-	-
Mn@Co_3O_4-3	537.675	97.002	547.178	303.748

Crystal Density (g/cm^3)				
Samples	**Co_3O_4**	**$CoMnO_3$**	**$MnCo_2O_4$**	**Mn_3O_4**
Co_3O_4	6.043	-	-	-
Mn@Co_3O_4-1	5.997	-	4.27	-
Mn@Co_3O_4-2	5.973	5.538	-	-
Mn@Co_3O_4-3	5.949	5.542	4.246	5.003

Lattice parameters (Å)				
		a	***B***	***c***
Co_3O_4	Co_3O_4	8.089	8.089	8.089
Mn@Co_3O_4-1	Co_3O_4	8.110	8.110	8.110
	$MnCo_2O_4$	8.164	8.164	8.164
Mn@Co_3O_4-2	Co_3O_4	8.121	8.121	8.121
	$CoMnO_3$	5.406	5.406	5.406
Mn@Co_3O_4-3	Co_3O_4	8.132	8.132	8.132
	$CoMnO_3$	5.408	5.408	5.408
	$MnCo_2O_4$	8.179	8.179	8.179
	Mn_3O_4	5.723	5.723	9.275

S.1.2. X-ray photoelectron spectroscopy

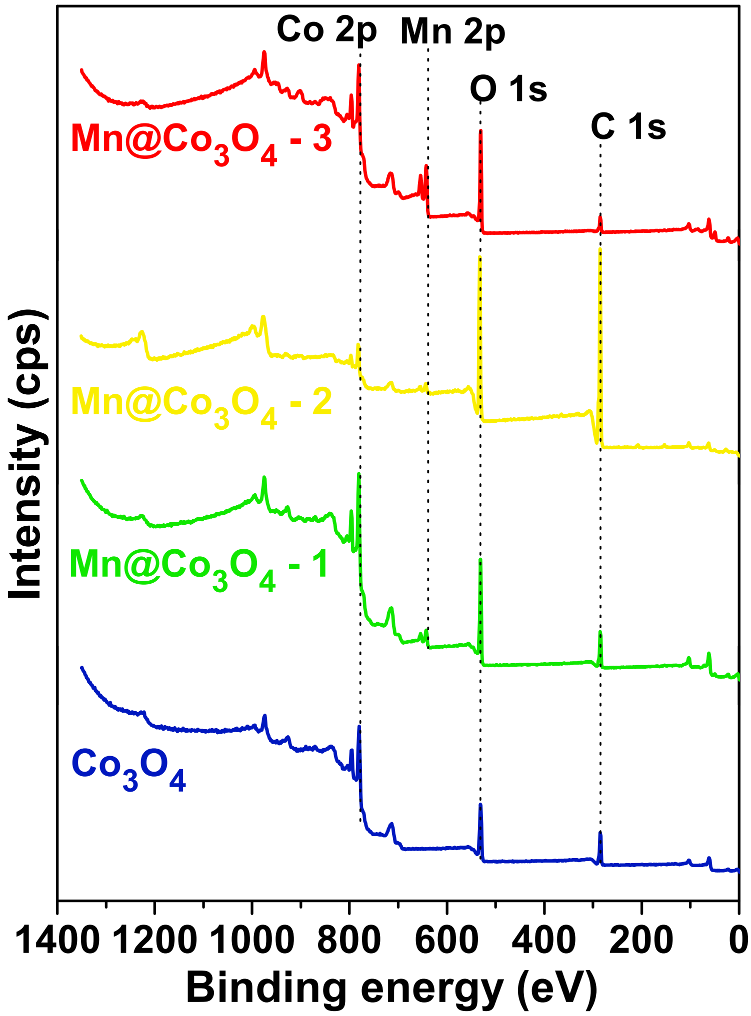

Figure S2. Survey spectra obtained for all catalysts.

Table S2. XPS data for: Mn@Co_3O_4-1, Mn@Co_3O_4- and Co_3O_4.

Catalyst	Binding Energy (eV)							
	$O_{lattice}$[(a)]	O_{ads}[(a)]	Co 2p Sat. 1[(b)]	Co 2p Sat. 2[(b)]	Co 2p Sat. 3[(b)]	Co 2p $\Delta(2p_{3/2} - 2p_{1/2})$ [(b)]	Mn 2p $\Delta(2p_{3/2} - 2p_{1/2})$ [(c)]	**(Mn+Co)/O**[(d)]
Mn@Co_3O_4-3	530.1	531.7	785.0	789.7	803.1	15.0	11.7	0.76
Mn@Co_3O_4-2	530.9	532.5	784.5	790.5	804.0	15.1	11.7	0.21
Mn@Co_3O_4-1	530.6	532.4	785.4	790.2	803.6	15.1	11.7	0.68
Co_3O_4	530.3	532.5	784.9	789.5	803.2	15.2	-	0.42

(a) Determined by high resolution spectra of O 1s.
(b) Determined by high resolution spectra of Co 2p.
(c) Determined by high resolution spectra of Mn 2p
- Estimated by the methodology proposed by Li and coworkers[R1]
- Not detected.

S.1.3. Thermogravimetric analysis

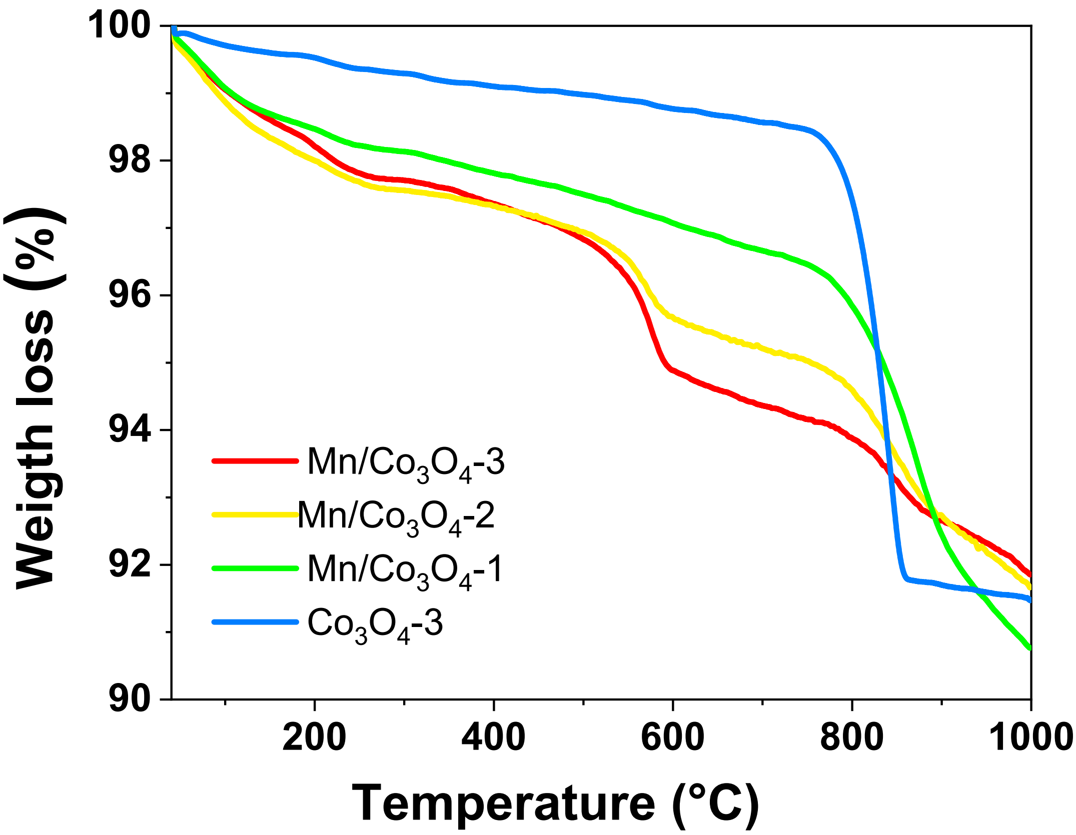

Fig. S3. TG curves of the catalysts (from 25 to 1000 ºC at 10 ºC min^{-1} of heating rate under helium flow of 50 mL min^{-1}).

The thermal behavior and stability of the samples were verified using thermogravimetric analysis (TG) under an inert atmosphere, as can be seen in **Fig. S3**. TG curves exhibited three weight loss steps for Co_3O_4: in the first region at 90 – 250 °C it was observed the humidity release of 0.6wt%, and in the second region from 720 to 740 °C the weight loss of 0.8wt% corresponded to the reduction of Co_3O_4 to CoO. The last event in the region 760 – 860 °C showed faster and major weight loss of about 6.8wt%, which corresponded to the reduction of the cobalt oxides CoO to Co(0). The three events are befitting with the literature.[R2] Reduction of cobalt oxide to metallic cobalt is difficult but is likely to occur according to the proposed reactions below.

$2\ Co_3O_4 \rightarrow 6\ CoO + O_2$ **(eq. 8)**

$2\ CoO \rightarrow 2Co + O_2$ **(eq. 9)**

Mn@Co_3O_4-1, Mn@Co_3O_4-2 and Mn@Co_3O_4-3 samples presented the same events described for and **Co_3O_4**, but with different weight losses corresponding to the different phases. However, less than 10wt% of weight was lost up to 1000 ^{o}C, indicating the overall high thermal stability of all catalysts.

S.1.4. Scanning electronic microscopy

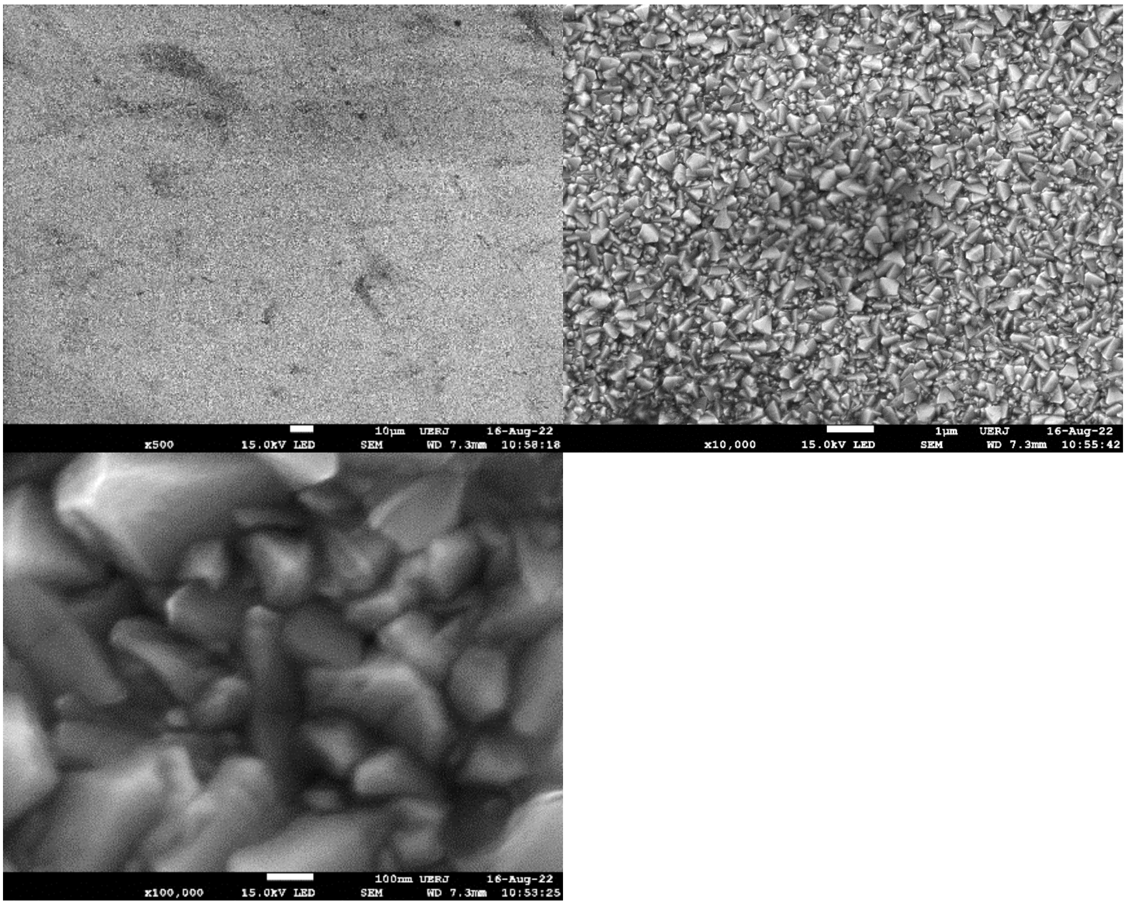

Fig. S4. FESEM images of pure FTO glass plate.

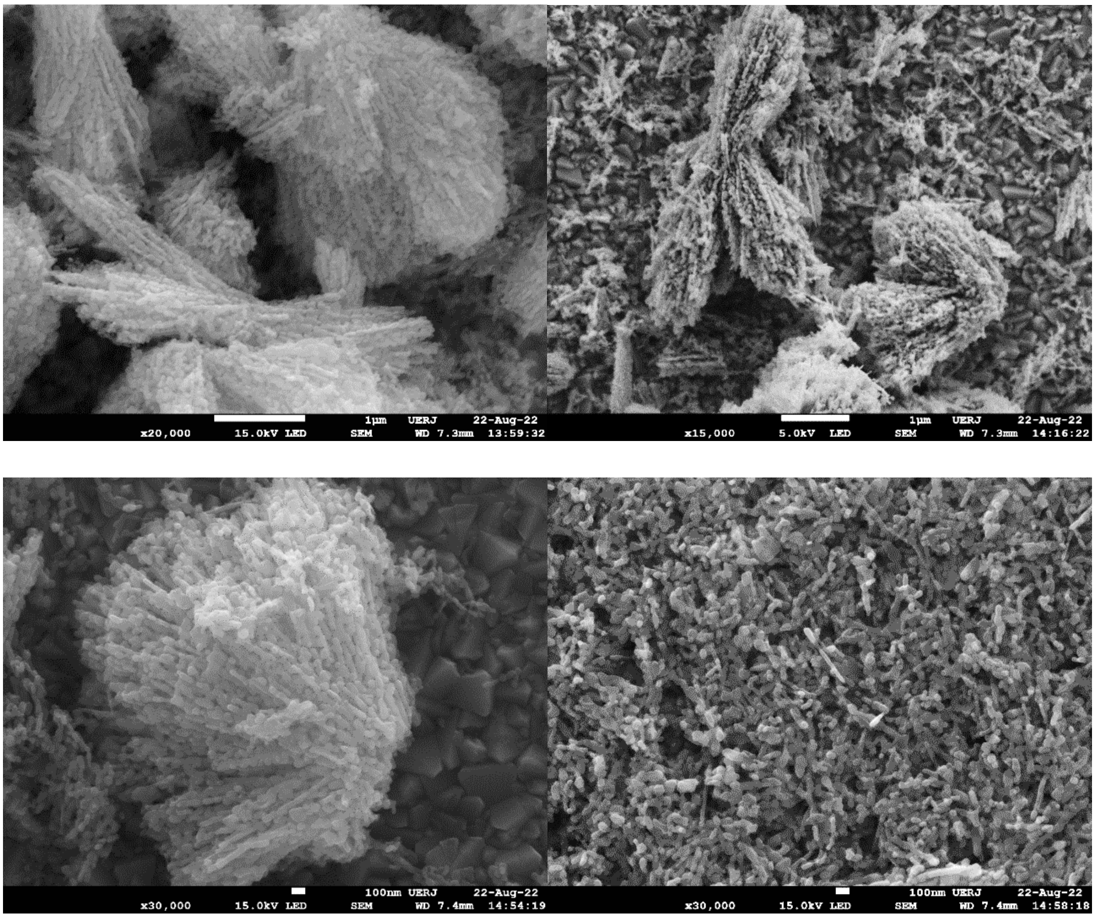

Fig. S5. FESEM images of Co_3O_4.

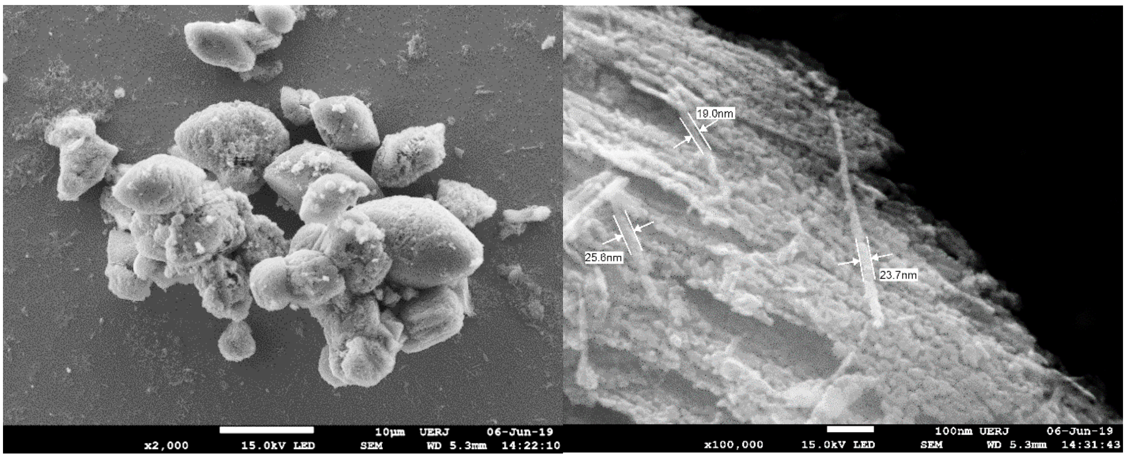

Fig. S6. FESEM images of $Mn@Co_3O_4$-1.

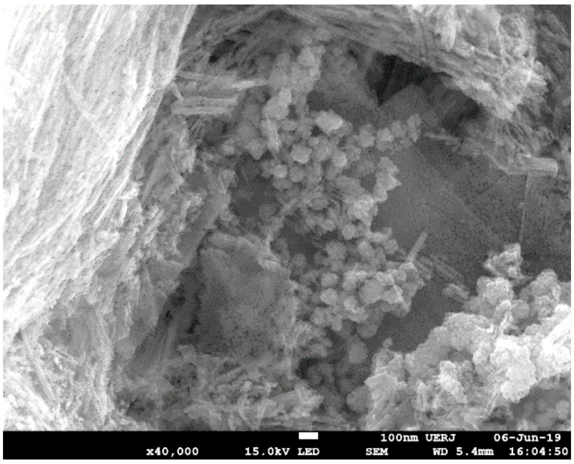

Fig. S7. FESEM images of Mn@Co_3O_4-2.

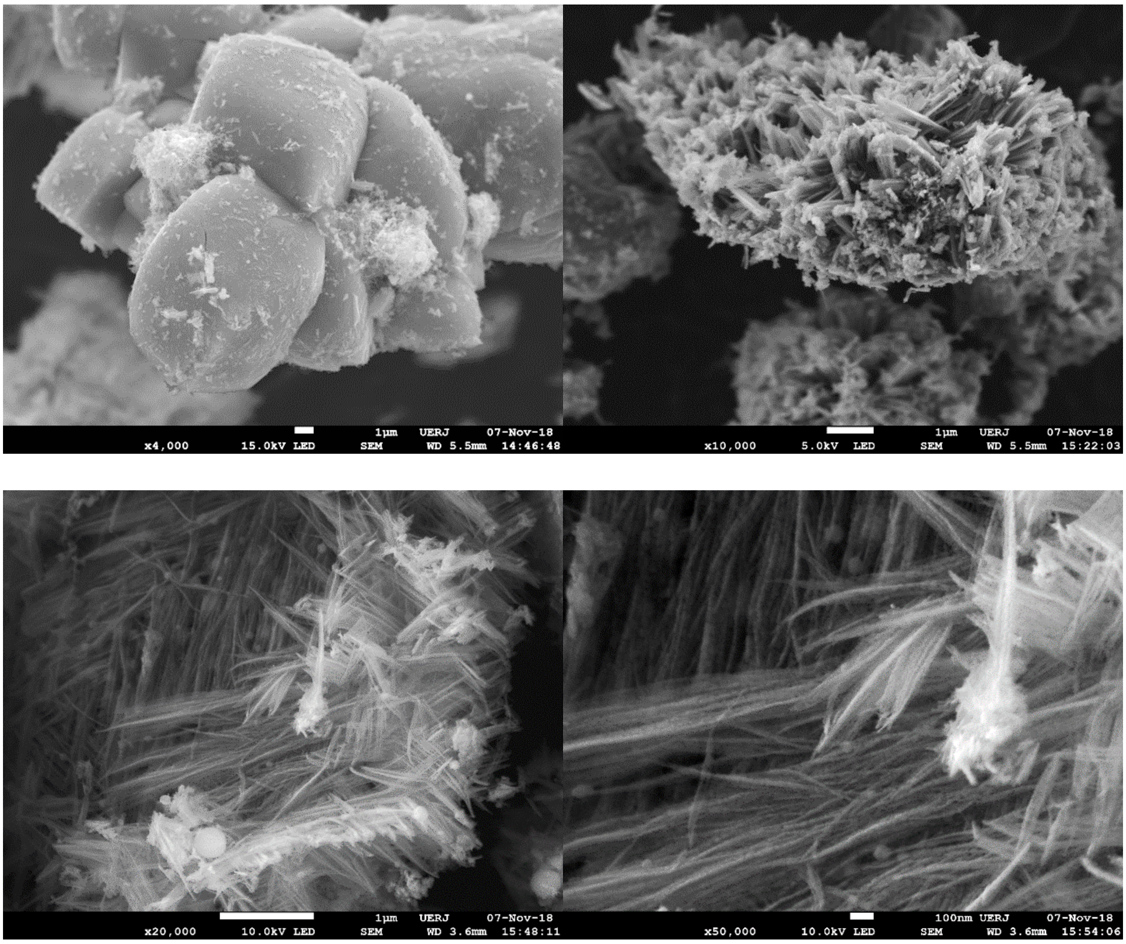

Fig. S8. FESEM image of Mn@Co_3O_4-3.

S.1.5. Cyclic voltammetry

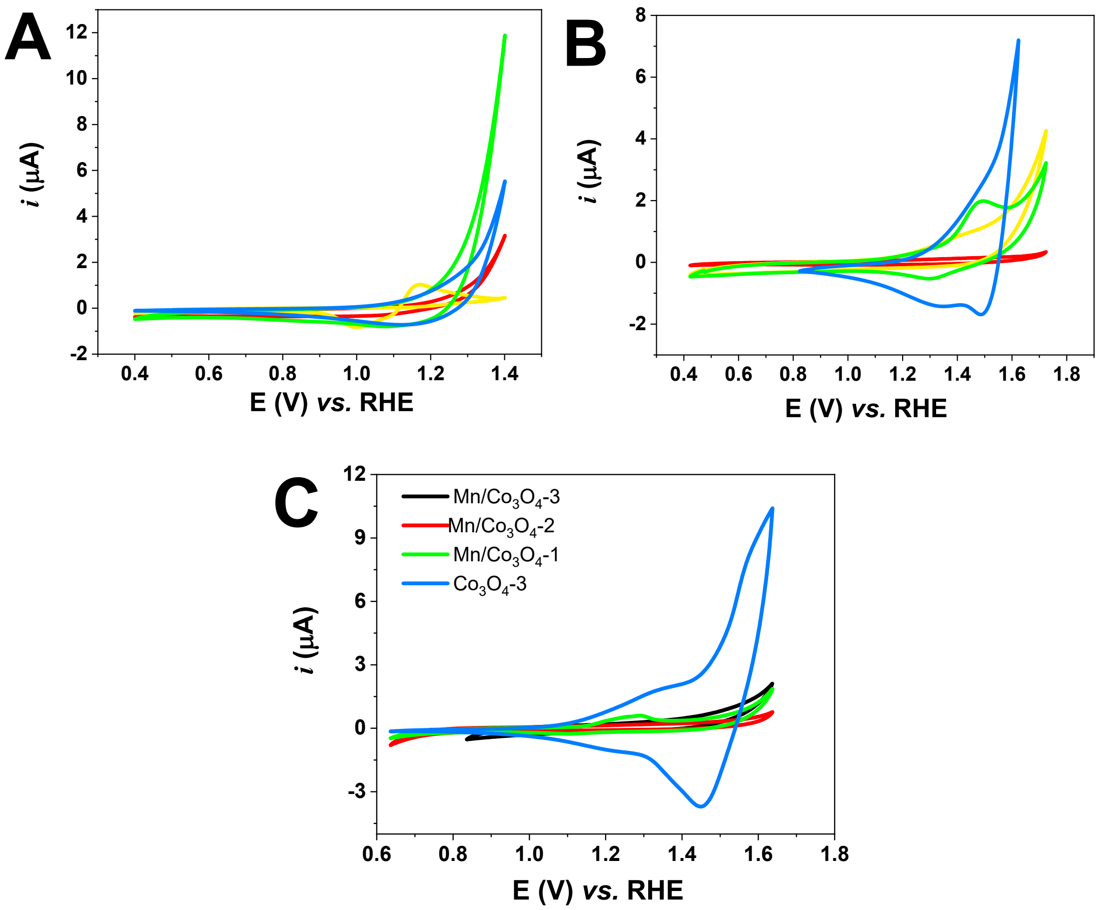

Figure S9. Cyclic voltammetry of the catalysts films: a) 0.1 mol L^{-1} HNO_3 pH 1, b) 0.1 mol L^{-1} Na_2SO_4 pH 7and c) 0.1 mol L^{-1} NaOH pH 13 with a scan rate of 50 mV s^{-1}.

S.1.6. Electrochemical impedance spectroscopy

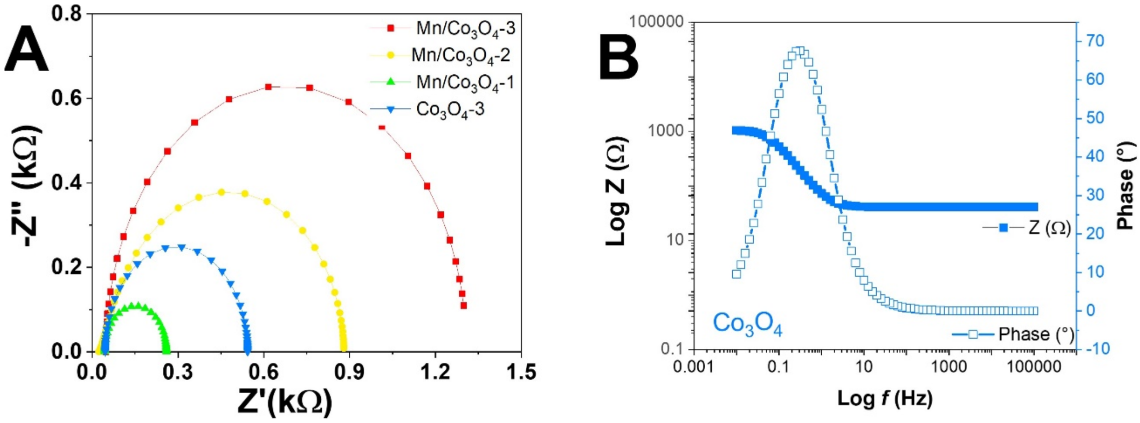

Figure S10. EIS measurements. (a) Nyquist diagram of the Mn@Co_3O_4-1, Mn@Co_3O_4-2, and Co_3O_4, (b) Bode plots for Co_3O_4 in 0.1 M HNO_3 pH 1.

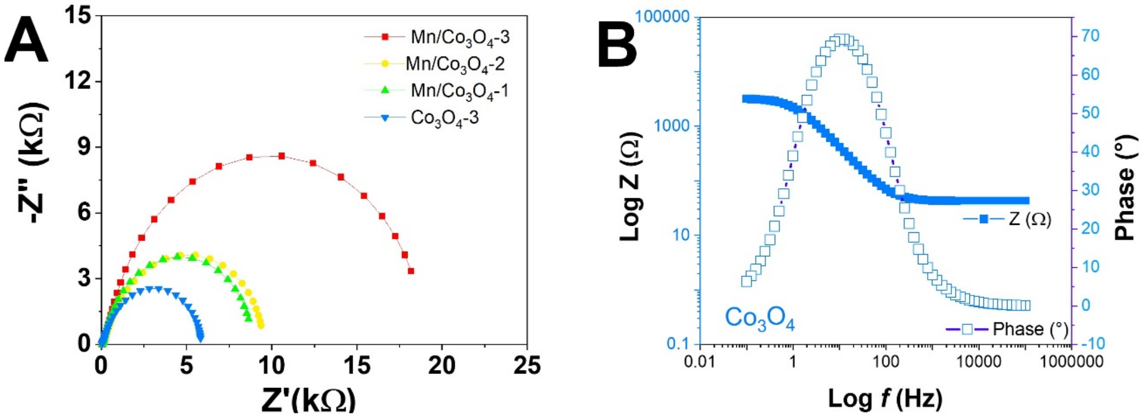

Figure S11. EIS measurements. (a) Nyquist diagram of the Mn@Co_3O_4-1, Mn@Co_3O_4-2, and Co_3O_4, (b) Bode plots for Co_3O_4 in 0.1 M Na_2SO_4 pH 7.

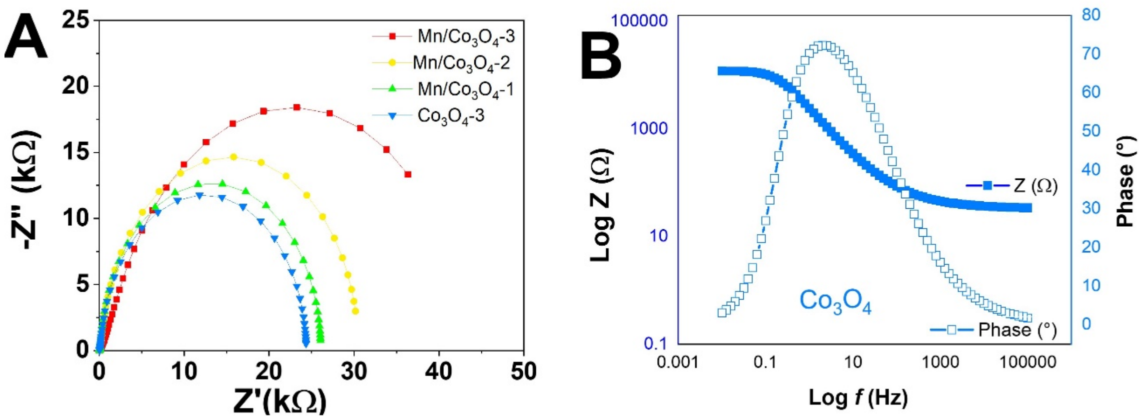

Figure S12. EIS measurements. (a) Nyquist diagram of the Mn@Co_3O_4-1, Mn@Co_3O_4-2, and Co_3O_4, (b) Bode plots for Co_3O_4 in 0.1 M NaOH pH 13.

Table S3. Values for charge transfer (R_{ct}) and electrochemical (R_s) resistances and Constant phase element (CPE) determined from electrochemical impedance spectroscopy.

Samples	pH	R_s (Ω cm²)	R_{ct} (Ω cm²)	CPE
Co_3O_4	1	39	543	0.96
Mn@Co_3O_4-1		34	879	0.98
Mn@Co_3O_4-2		38	259	0.97
Mn@Co_3O_4-3		37	1301	0.98
Co_3O_4	7	50	2613	0.96
Mn@Co_3O_4-1		53	3170	0.91
Mn@Co_3O_4-2		55	4431	0.99
Mn@Co_3O_4-3		55	19233	0.97
Co_3O_4	13	63	12004	0.99
Mn@Co_3O_4-1		65	26047	0.98
Mn@Co_3O_4-2		64	24339	0.95
Mn@Co_3O_4-3		66	45390	0.99

S.2. Oxygen evolution reaction electrocatalysis

S.2.1. Linear sweep voltammetry curves using FTO as working electrode

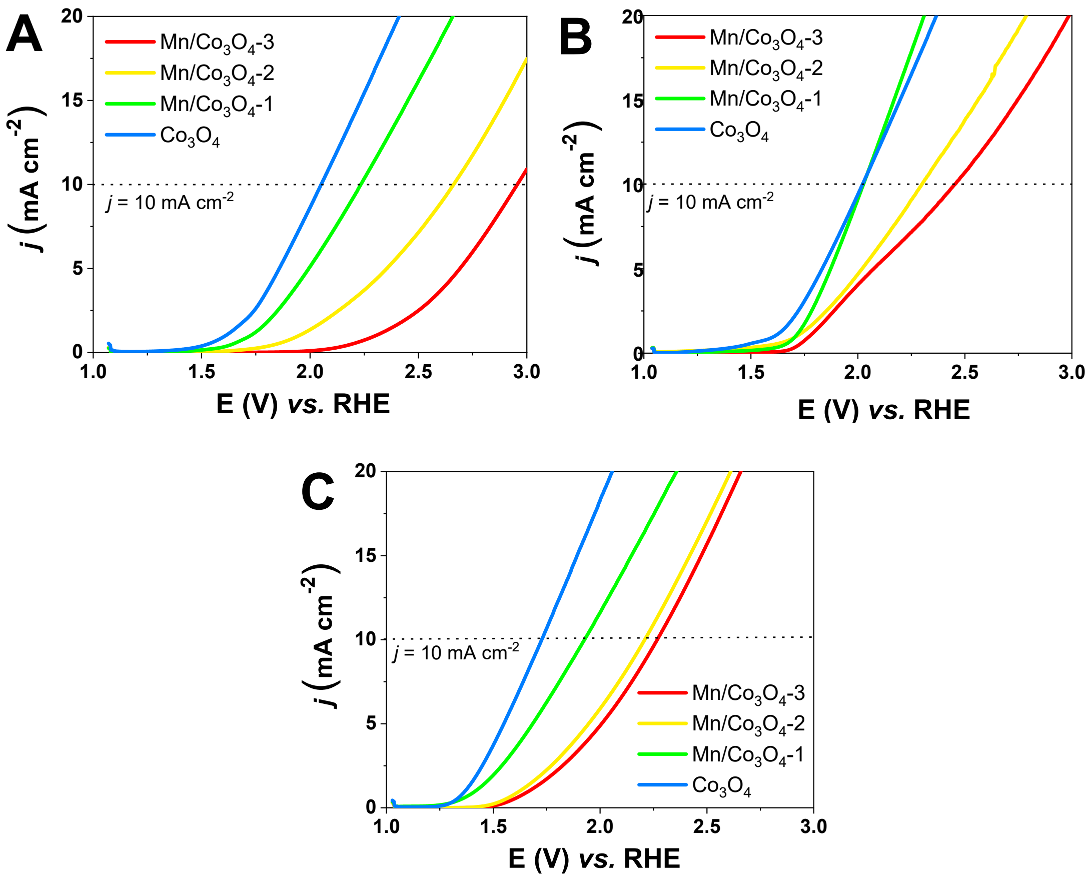

Fig. S13. Polarization curves for oxygen evolution reactions of the catalysts films FTO electrode: a) LSV curves in 0.1 mol L^{-1} HNO_3 pH 1, c) LSV curves in 0.1 mol L^{-1} Na_2SO_4 pH 7, e) LSV curves in 1.0 mol L^{-1} NaOH pH 14, b) Tafel plots in pH 1, d) Tafel plots in pH 7 and f) Tafel plots in pH 14 with a scan rate of 0.005 Vs^{-1}.

Table S4. OER electrocatalytic data: η_{10} (mV) at j = 10 mA/cm², TOF_{450} (s^{-1}) at η = 450 mV, using FTO modified electrode.

Catalyst	pH 1		pH 7		pH 14	
	η_{10}	TOF_{450}	η_{10}	TOF_{450}	η_{10}	TOF_{450}
Co_3O_4	810	3.20×10^{-3}	780	3.47×10^{-3}	490	1.69×10^{-2}
Mn@Co_3O_4-1	990	1.39×10^{-3}	790	1.33×10^{-3}	680	9.75×10^{-3}
Mn@Co_3O_4-2	1420	3.57×10^{-4}	1006	1.31×10^{-3}	960	2.84×10^{-3}
Mn@Co_3O_4-3	1719	1.13×10^{-4}	1210	4.29×10^{-4}	1030	1.96×10^{-3}

Table S5. OER electrocatalytic TOF_{450}/S_{BET} (s^{-1} g m^{-2}) at η = 450 mV.

Catalyst	pH 1	pH 7	pH 14
	FTO		
Co_3O_4	2.10×10^{-4}	2.28×10^{-4}	1.11×10^{-3}
Mn@Co_3O_4-1	2.11×10^{-5}	2.01×10^{-5}	1.48×10^{-4}
Mn@Co_3O_4-2	6.71×10^{-6}	2.46×10^{-5}	5.34×10^{-5}
Mn@Co_3O_4-3	1.84×10^{-6}	7.00×10^{-6}	3.20×10^{-5}
	RDE		
Co_3O_4	9.07×10^{-6}	2.99×10^{-4}	6.67×10^{-3}
Mn@Co_3O_4-1	1.37×10^{-6}	5.65×10^{-6}	5.02×10^{-4}
Mn@Co_3O_4-2	1.09×10^{-6}	1.06×10^{-5}	4.79×10^{-4}
Mn@Co_3O_4-3	7.87×10^{-7}	4.23×10^{-5}	2.19×10^{-4}

Table S6. OER electrocatalytic data: TOF (s^{-1}) at $\eta = 450$ mV, considering only the Co_3O_4 content in the oxide as active catalyst phase.

Catalyst	Phase (wt%)	pH 1	pH 7	pH 14
		FTO		
Co_3O_4	100	3.20×10^{-3}	3.47×10^{-3}	1.69×10^{-2}
Mn@Co_3O_4-1	97.0	1.43×10^{-3}	1.37×10^{-3}	1.01×10^{-2}
Mn@Co_3O_4-2	82.8	4.31×10^{-4}	1.58×10^{-3}	3.43×10^{-3}
Mn@Co_3O_4-3	46.8	2.42×10^{-4}	9.17×10^{-4}	4.20×10^{-3}
		RDE		
Co_3O_4	100	1.38×10^{-4}	4.54×10^{-3}	1.01×10^{-1}
Mn@Co_3O_4-1	97.0	9.31×10^{-5}	3.84×10^{-4}	3.41×10^{-2}
Mn@Co_3O_4-2	82.8	6.98×10^{-5}	6.78×10^{-4}	3.08×10^{-2}
Mn@Co_3O_4-3	46.8	1.03×10^{-4}	5.54×10^{-3}	2.87×10^{-2}

Table S7. OER electrocatalytic data: TOF_{450}/S_{BET} (s^{-1} g m^{-2}) at η = 450 mV, considering only the Co_3O_4 content in the oxide as active catalyst phase.

Catalyst	Phase (wt%)	pH 1	pH 7	pH 14
		FTO		
Co_3O_4	100	2.10×10^{-4}	2.28×10^{-4}	1.11×10^{-3}
Mn@Co_3O_4-1	97.0	2.17×10^{-5}	2.07×10^{-5}	1.53×10^{-4}
Mn@Co_3O_4-2	82.8	8.10×10^{-6}	2.97×10^{-5}	6.44×10^{-5}
Mn@Co_3O_4-3	46.8	3.94×10^{-6}	1.50×10^{-5}	6.84×10^{-5}
		RDE		
Co_3O_4	100	9.07×10^{-6}	2.99×10^{-4}	6.67×10^{-3}
Mn@Co_3O_4-1	97.0	1.41×10^{-6}	5.82×10^{-6}	5.18×10^{-4}
Mn@Co_3O_4-2	82.8	1.31×10^{-6}	1.28×10^{-5}	5.79×10^{-4}
Mn@Co_3O_4-3	46.8	1.68×10^{-6}	9.03×10^{-5}	4.69×10^{-4}

S.2.2. Tafel plots using FTO as working electrode

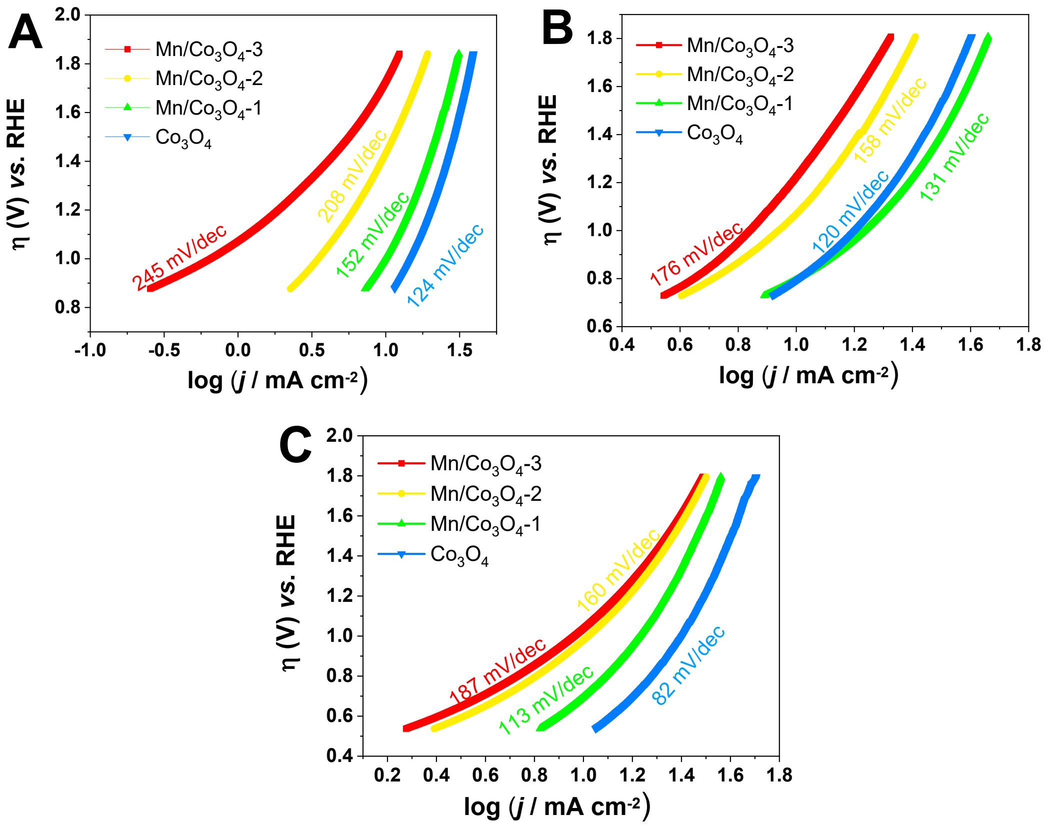

Fig. S14. Tafel plots for oxygen evolution reactions of the catalysts films FTO electrode in: a) pH 1, b) pH 7 and c) pH 13 with a scan rate of 5 mV s^{-1}.

Table S8. Tafel slope for OER electrocatalytic activity in FTO electrode.

Catalyst	pH 1	pH 7	pH 13
	Tafel Slope ($mV\ dec^{-1}$)	**Tafel Slope ($mV\ dec^{-1}$)**	**Tafel Slope ($mV\ dec^{-1}$)**
Co_3O_4	128	120	82
Mn@Co_3O_4-1	208	158	160
Mn@Co_3O_4-2	152	131	113
Mn@Co_3O_4-3	245	176	187

Table S9. Comparison of OER catalytic activity of prepared catalyst with that of other recently reported, transition metal-based catalysts.

Catalyst	pH	Current Density ($mA\ cm^{-2}$)	Overpotential (mV)	Tafel Slope ($mV\ dec^{-1}$)	Refs.
Mn@Co_3O_4-1	1	10	752	121	This work
Mn@Co_3O_4-1	7	10	673	109	This work
Mn@Co_3O_4-1	14	10	320	52	This work
5%Mn-Co	13	10	1630	82	Song,2016[R3]
10%Mn-Co	13	10	1630	99	Song,2016[R3]
10%Mn-Co	13	10	1630	100	Song,2016[R3]
20%Mn-Co	13	10	1650	114	Song,2016[R3]
Mn_3O_4	14	3	600	60	Hirai,2016[R4]
$Mn_{2.4}Co_{0.6}O_4$	14	3	510	51	Hirai,2016[R4]
$Mn_{2.1}Co_{0.9}O_4$	14	3	590	31	Hirai,2016[R4]
Co_3O_4 nanorods	4	6.5	389	120	Ramsundar,2015[R5]
Co_3O_4 nanorods	7	10	606	200	Ramsundar,2015[R5]
Co_3O_4 nanorods	7	3.7	385	70	Ramsundar,2015[R5]
Co_3O_4 nanocube	13	10	400	60	Chen,2015[R6]
Co_3O_4 layer	14	10	203	63	Zhang,2019[R7]
Y-α-$Co(OH)_2$	13	1	329	59	Bose,2017[R8]
$MnCo_2O_4$/CC	7	10	403	197	Hao,2017[R9]
$(Co_{2.7}Mn_{0.3})O_4$	14	10	490	35.8	Park,2019[R10]
Co_3O_4	14	10	368	75.5	Lankauf,2020[R11]

$MnCo_2O_4$ (Co_3O_4 + $Mn_{1.4}Co_{1.6}O_4$)	14	10	327	78.9	Lankauf,2020[R11]
$MnCo_2O_4$	14	10	365	50.60	Park,2020[R12]
Co_3O_4 + α-MnO_2 Powder blend	13	10	370	129	Fink,2020[R13]

S.3. Electrocatalysts characterization after oxygen evolution reaction

S.3.1. Scanning electronic microscopy

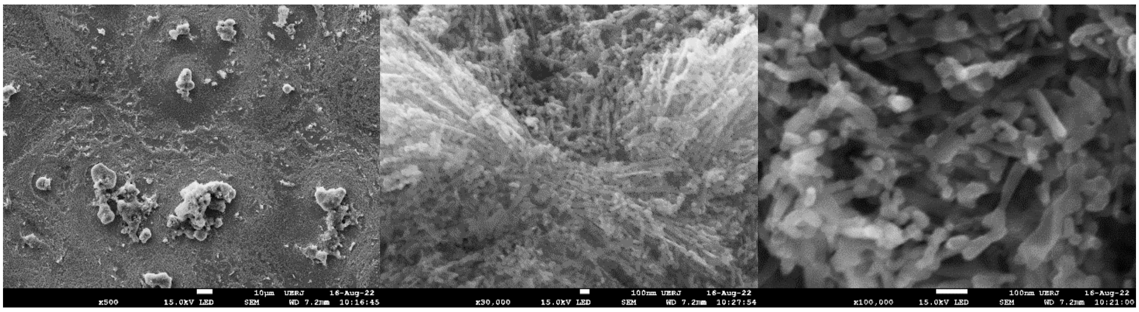

Fig. S15. FESEM images of Co_3O_4 after OER at pH 1.

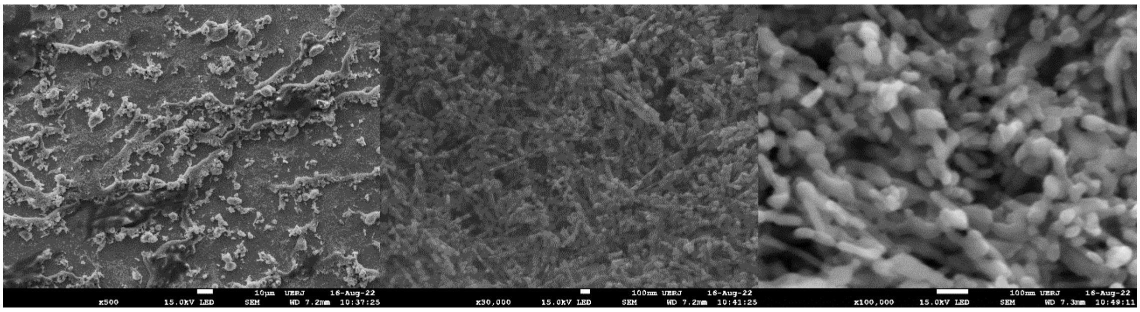

Fig. S16. FESEM images of Co_3O_4 after OER at pH 7.

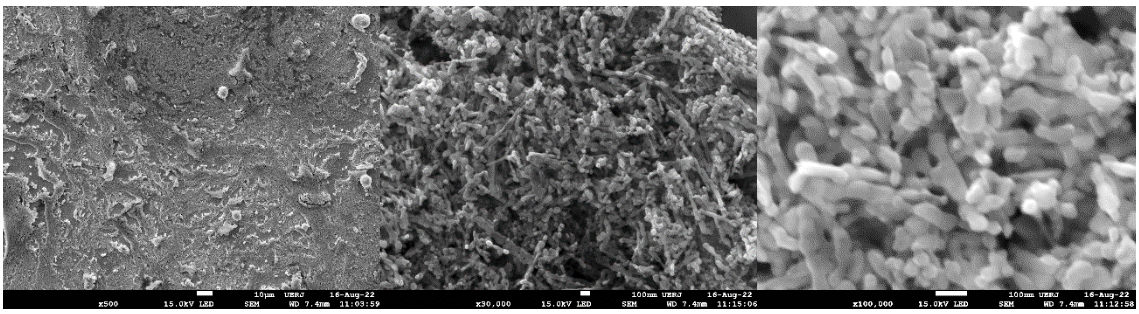

Fig. S17. FESEM images of Co_3O_4 after OER at pH 14.

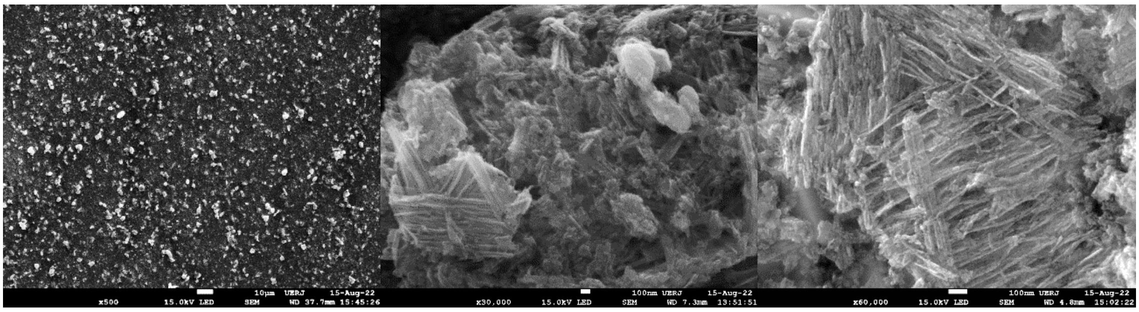

Fig. S18. FESEM images of Mn@Co_3O_4-3 after OER at pH 1.

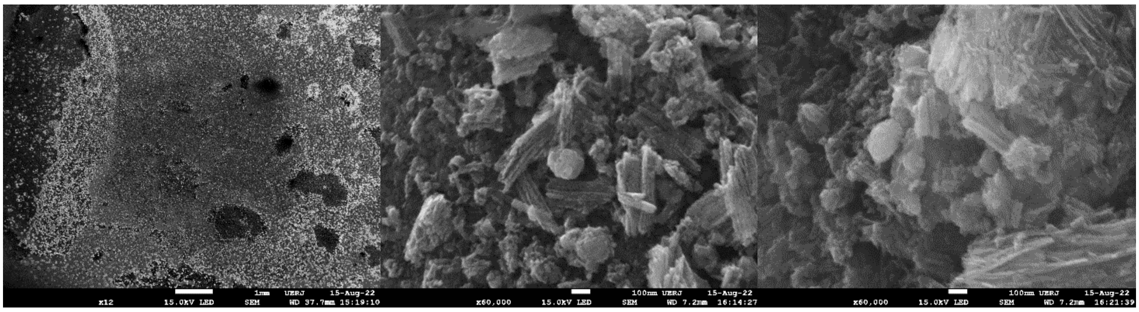

Fig. S19. FESEM images of Mn@Co_3O_4-3 after OER at pH 7.

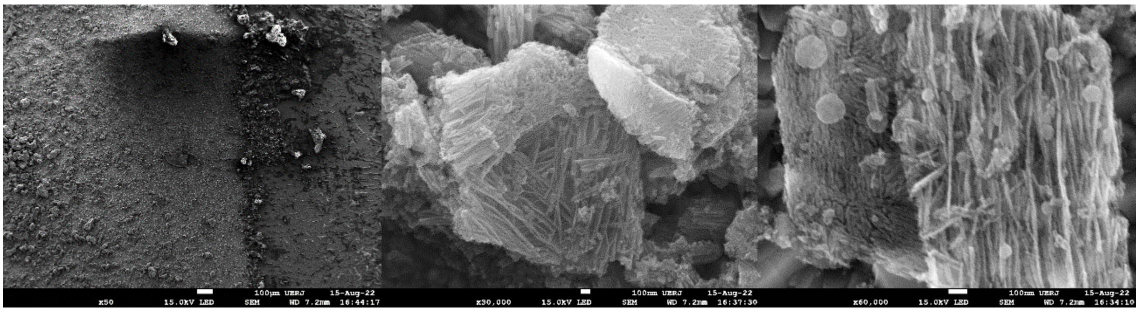

Fig. S20. FESEM images of Mn@Co_3O_4-3 after OER at pH 14.

S.3.2. Raman spectroscopy

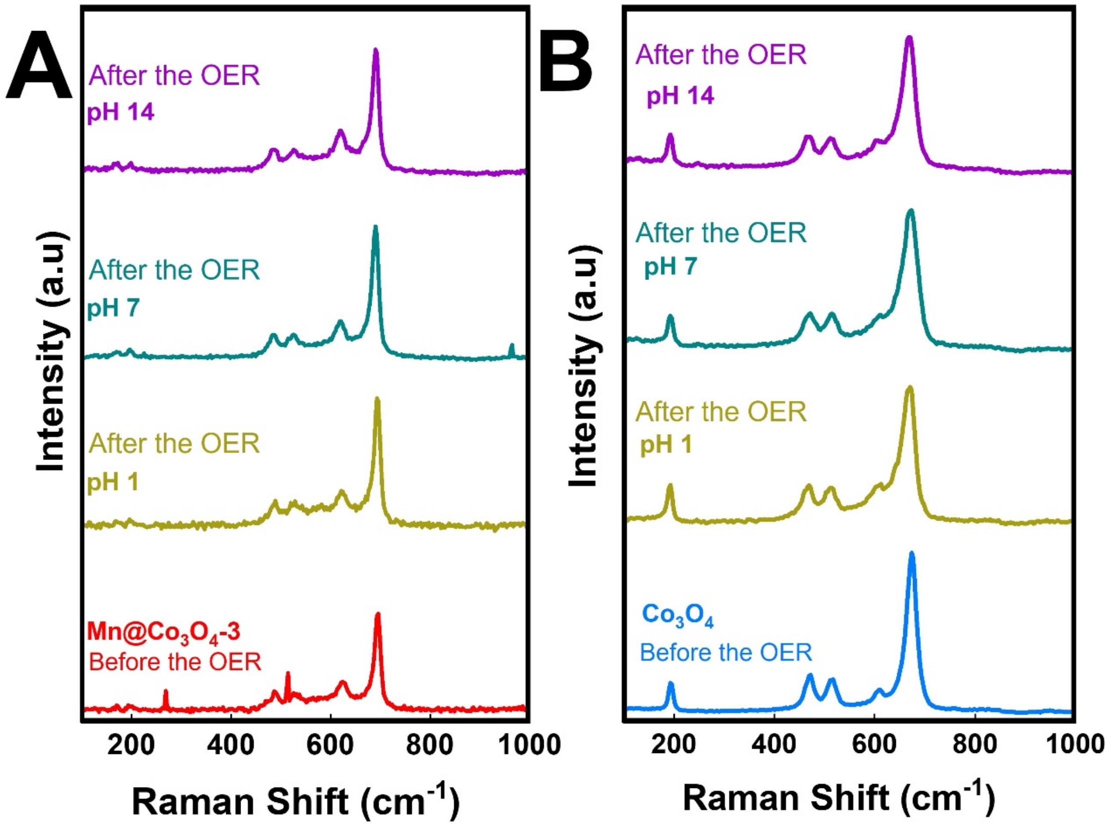

Figure S21. Raman spectra of the FTO films of the (A) Mn@Co_3O_4 and (B) Co_3O_4 before and after the OER for all pHs.

References

R1 K. Li, R. Zhang, R. Gao, G. Q. Shen, L. Pan, Y. Yao, K. Yu, X. Zhang and J. J. Zou, *Applied Catalysis B: Environmental*, 2019, **244**, 536–545.

R2 Y. K. Kim, S. I. Cha and S. H. Hong, *Journal of Materials Chemistry A*, 2013, **1**, 9802–9808.

R3 W. Song, Z. Ren, S. Y. Chen, Y. Meng, S. Biswas, P. Nandi, H. A. Elsen, P. X. Gao and S. L. Suib, *ACS Applied Materials and Interfaces*, 2016, **8**, 20802–20813.

R4 S. Hirai, S. Yagi, A. Seno, M. Fujioka, T. Ohno and T. Matsuda, *RSC Advances*, 2016, **6**, 2019–2023.

R5 R. M. Ramsundar, J. Debgupta, V. K. Pillai and P. A. Joy, *Electrocatalysis*, 2015, **6**, 331–340.

R6 Z. Chen, C. X. Kronawitter and B. E. Koel, *Physical Chemistry Chemical Physics*, 2015, **17**, 29387–29393.

R7 H. Zhang, J. Zhang, Y. Li, H. Jiang, H. Jiang and C. Li, *Journal of Materials Chemistry A*, 2019, **7**, 13506–13510.

R8 S. Bose, J. Debgupta, R. M. Ramsundar and S. K. Das, *Chemistry - A European Journal*, 2017, **23**, 8051–8057.

R9 S. Hao and Y. Yang, *Journal of Materials Chemistry A*, 2017, **5**, 12091–12095.

R10 K. R. Park, J. E. Jeon, G. Ali, Y.-H. Ko, J. Lee, H. Han and S. Mhin, *Catalysts*, 2019, **9**, 564.

R11 K. Lankauf, K. Cysewska, J. Karczewski, A. Mielewczyk-Gryń, K. Górnicka, G. Cempura, M. Chen, P. Jasiński and S. Molin, *International Journal of Hydrogen Energy*, 2020, **45**, 14867–14879.

R12 K. R. Park, J. E. Jeon, K. Kim, N. Oh, Y. H. Ko, J. Lee, S. H. Lee, J. H. Ryu, H. S. Han and S. Mhin, *Applied Surface Science*, 2020, **510**, 145390.

R13 C. R. Michael F. Fink, Julia Eckhardt, Prashant Khadke, Thorsten Gerdes, *ChemElectroChem*, 2020, 7, 4822–4836.